Journal of Energy Storage 72 (2023) 108593

Contents lists available at ScienceDirect

Journal of Energy Storage

journal homepage: www.elsevier.com/locate/est

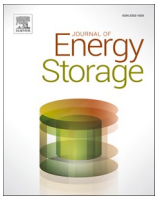

Research Papers

Oxygen-less electrodes for stability enhancement of vanadium non-aqueous redox flow batteries

Kashif Mushtaq [a,b,c], Sofia Delgado [a,b], Adélio Mendes [a,b,*]

[a] LEPABE – Laboratory for Process Engineering, Environment, Biotechnology and Energy, Faculty of Engineering, University of Porto, Rua Dr. Roberto Frias, Porto, Portugal
[b] ALiCE – Associate Laboratory in Chemical Engineering, Faculty of Engineering, University of Porto, Rua Dr. Roberto Frias, Porto, Portugal
[c] Presently at Iberian Center for Research in Energy Storage, CIIAE, Cáceres, Spain

ARTICLE INFO

Keywords:
Oxygen-less electrodes
Electrode treatment
Non-aqueous redox flow battery
Hydrogen reduction
Carbon felt

ABSTRACT

A meticulous study was conducted to investigate the capacity loss and degradation of non-aqueous vanadium flow batteries. It was observed that the presence of moisture and oxygen in the system triggers a parasitic reaction leading to the formation of irreversible $VO(acac)_2$, which hampers high-performance operation. The main source of this issue was identified as oxygen-rich electrodes commonly used in these batteries. To address this challenge, a novel approach was employed to modify the surface of carbon felt electrodes through hydrogen reduction thermal treatment, effectively mitigating the concentration of oxygen functional sites. The electrodes of carbon felt were treated at 700 °C with hydrogen greatly reduced the oxygen content in the electrodes, leading to increased reaction rate constants and reduced overall system impedance. The thermal treatment under a reducing atmosphere successfully mitigated the degradation mechanisms and extended the device's lifespan. The battery equipped with these modified electrodes demonstrated a storage capacity of 521 mAh l^{-1} over 45 charge/discharge cycles, representing the highest reported stability. Moreover, the maximum current density was improved by 60 % compared to the system using pristine electrodes. Morphological analysis was conducted alongside electrochemical testing to evaluate the performance of the modified electrodes. This technique paves the way to a closer level toward pilot-scale commercialization.

1. Introduction

The transition toward a climate-neutral society requires fundamental modifications in the way energy is being transformed, stored, and used. This motivates the increasing trend for the implementation of renewable energy systems and electric battery vehicles (EBV) encouraging the development of energy storage systems, mainly batteries. The EU's total CO_2 footprint in 2019 reached 6.7 tons per person, according to Eurostat [1]. Unsurprisingly, the amount of battery demand increased to 280 GWh between 2010 and 2021, growing by 30 % annually [2]. This trend is anticipated to continue increasing at a projected rate of 25 % yearly, reaching a volume of 2035 GWh by 2030. Still, to reach the sustainability goals set by the European Green Deal, batteries must exhibit ultra-high performance surpassing from present-day [2].

Lithium-ion chemistries are dominating the market in the domain of high-energy-density rechargeable batteries. However, the present generation of Li-ion batteries (LIBs) is approaching their performance limits. Now without a breakthrough, battery performance, and production will not keep up with the massive energy demand required to fulfill the objectives of a climate-neutral society. While LIBs will continue to play a major role in the energy storage landscape, alternative technologies are required for enabling the creation of future sustainable batteries and lay the foundation for European competitiveness during the energy transition. Recent studies projected the lowest levelized cost of storage (LCOS) for nine electricity storage technologies from 2015 to 2050; the top two technologies are LIBs and redox flow batteries (RFB) [3].

One of the major challenges concerning RFB technology refers to its inherently low energy density. The highest reported energy density attained for an aqueous VRFB was solely 52.26 Wh l^{-1} when employing 3 M, which is the maximum vanadium concentration in solution, before its precipitation [4]. Other battery types, such as Li-ion, NiMH, Ni-Cd, *etc.*, deliver volumetric energy densities above 100 Wh l^{-1} at the lab scale. The energy density may be enhanced by increasing the concentration of redox species, increasing the cell voltage by introducing redox

* Corresponding author and Professor at: LEPABE, Faculty of Engineering, University of Porto, Rua Dr. Roberto Frias, 4200-465 Porto, Portugal.
E-mail addresses: up201502472@fe.up.pt (K. Mushtaq), sdelgado@fe.up.pt (S. Delgado), mendes@fe.up.pt (A. Mendes).

https://doi.org/10.1016/j.est.2023.108593
Received 31 March 2023; Received in revised form 16 July 2023; Accepted 31 July 2023
Available online 19 August 2023

species having higher redox potential differences, or increasing the number of participating electrons in the reaction [5]. This relationship is governed by the following equation:

$$\text{Energy density} = \frac{1}{2} n C^{O} E_{CELL} \quad (1)$$

where, n is the number of exchanged electrons, C^{O} is the solubility of the redox species, E_{CELL} is the cell potential difference. The option of increasing the concentration of vanadium in the aqueous electrolyte is no longer a possibility since the solubility limit has already been reached. Since the water-splitting reaction occurs at the potential difference of 1.23 V *vs.* RHE (at acidic pH = 1, T_{atm} = 25 °C, P_{atm} = 1 bar) any further increase in the operating cell voltage of the aqueous-based battery is hindered as it leads to side reactions *i.e.* evolution of both hydrogen and oxygen gases.

The development of polyoxometalate-based RFBs emerged as a route for boosting the energy density of aqueous RFBs, by allowing the increment of the number of electrons transferred per molecule during the redox reaction [6]. However, most of the commercial versions of aqueous RFBs solely reach energy densities of 25 to 30 Wh l^{-1}. On the other hand, non-aqueous electrolytes, either composed of ionic liquids, deep eutectic solvents, or molecular organic solvents, allow to have a wider electrochemical stability window [7]. Through non-aqueous electrolytes, novel redox species can be taken into account which is commonly incompatible with aqueous electrolytes due to their low solubility, chemical reactivity, or redox potentials beyond the water stability window. Therefore, the wide variety of molecular solvents such as acetonitrile, propylene carbonate, DMSO, DMA, DMF, *etc.*, and supporting electrolytes such as $TEABF_4$, $TEAPF_6$, $TBAClO_4$, LiTFSI, *etc.*, appear promising for use in this application.

Vanadium-based non-aqueous redox flow batteries having vanadium acetylacetonate – $V(acac)_3$ – as redox species are being studied as model electrochemistry for non-aqueous versions of a redox flow battery [5]. The ability of this electrolyte to start the battery from the same valency state (V^{3+}) at both half cells makes it more appealing. Vanadium species are a good contender for future commercial versions of non-aqueous redox flow batteries because of their solubility in most organic solvents and their economical feasibility. The half-cell reactions of the vanadium-based non-aqueous electrochemistry, loaded with a solvent/supporting electrolyte of acetonitrile/$TEABF_4$, are given below in discharging direction [8]:

$$\left[V(IV)(acac)_3\right]^{+} + e^{-} \rightleftharpoons V(III)(acac)_3,\ E^{o} = 0.45\ V\ vs.\ Ag^{+}/Ag \quad (2)$$

$$V(III)(acac)_3 + e^{-} \rightleftharpoons \left[V(II)(acac)_3\right]^{-},\ E^{o} = -1.75\ V\ vs.\ Ag^{+}/Ag \quad (3)$$

Despite the high cell voltage of this chemistry, 2.2 V, the electrolyte is very sensitive to moisture and oxygen, which triggers the parasitic side reactions [9]. These parasitic side reactions are responsible to consume the concentration of redox species which in turn contribute to the loss of capacity and operational current density. In the RFB, sources of moisture might arise from residual water on chemical reagents, solvents, or even from that absorbed in the components of the cell. Besides, a dry, inert atmosphere should be employed to protect the electrolyte from any environmental moisture. Nonetheless, it was observed that even maintaining the electrolyte in a fully inert atmosphere inside a glovebox is not adequate to maintain acceptable stability throughout the operation of the battery [9]. The sudden cell failure should then root in the components of the cell; the authors suspected carbon felts/bipolar plates as a possible source of oxygen since they normally display a surface containing a high concentration of oxygenated functional groups [10]. Several studies report the presence of oxygen-functional groups on the electrodes. Their presence is beneficial in the case of aqueous-based electrochemical systems, making the electrodes more hydrophilic and then facilitating the redox species to anchor for exchange charge [11,12].

As a strong reducing agent, hydrogen can be used to eliminate certain oxygen group functions. Therefore, the effects of various pretreatments on the shape and functionality of the carbon felts in a V-NAqRFB were evaluated in this work. Mainly, the effect of using pristine carbon felt electrodes from SGL (4.6 GFD) – referred to as P, oxygen treated electrodes – referred to as PO, hydrogen treated electrodes – referred to as PH, and a combination of oxygen followed by a hydrogen treated electrodes – referred to as POH, were studied. These electrodes were then characterized concerning the morphology and surface chemistry, by Scanning Electron Microscopy (SEM) and Fourier-transform infrared spectroscopy (FTIR), and concerning the electrochemical performance in a NAqRFB-cell, by performing impedance spectroscopy and polarization measurements. This study allowed us to decipher the connection between the surface chemistry of each electrode, the stability of the cell, and its corresponding electrochemical activity.

2. Experimental methods

2.1. Materials

Tetraethylammonium tetrafluoroborate, 99 %, $TEABF_4$ acquired from Alfa Aesar; vanadium(III) acetylacetonate, 97 %, $V(acac)_3$ acquired from Strem chemicals; and acetonitrile, anhydrous, 99.8 %, ACN, acquired from Sigma Aldrich were used as received.

Acetonitrile (ACN) as solvent and $TEABF_4$ as supporting electrolyte was used in all experiments. The electrolyte used for passing in the flow-cell was composed of ACN + $TEABF_4$ 0.5 M + $V(acac)_3$ 0.1 M, referred to in this study as A1. A lower concentrated electrolyte consisting of ACN + $TEABF_4$ 0.1 M + $V(acac)_3$ 0.02 M was used for the voltammetry studies and is referred to in this study as A2. The composite membrane consists of layers of the separator from Celgard and Nafion membrane in the order of C2500|Nafion HP|C2500 referred to as C25-HP-C25 in this study. The electrodes were purchased from Sigracell, SGL Carbon, 4.6 mm in thickness.

2.2. Preparation of the electrodes

Different heat and acid treatments were applied to as-received carbon felt samples, as indicated in Table 1.

2.3. Morphology characterization

The surface morphologies of the carbon felt electrodes were analyzed using a field emission scanning electron microscope SEM (PhenomPro

Table 1
Treatments applied to as-received electrodes.

Reference	Steps of preparation
Pristine (P)	Cleaning with ethanol and dried in the oven at 80 °C for 2 h
Pristine with thermal treatment in O_2 environment (PO)	Boiled in 1 M H_2SO_4 for 12 h. DI water was used for washing and then dried in an oven for 2 h at 120 °C. Placed inside a furnace for 10 h at 400 °C using an oxygen-rich environment. Reached the room temperature inside the furnace.
Pristine with thermal treatment in H_2 environment at 400 °C/700 °C (PH/PH2)	Cleaning with ethanol and dried in an oven at 80 °C for 2 h. Placed in a tube furnace under a hydrogen flow rate of 190 ml min^{-1} for 10 h at 400 °C (for PH2, temperature = 700 °C). Reached the room temperature inside the furnace.
Pristine with thermal treatment in O_2 followed by H2 (POH/POH2)	PO samples were placed in a tube furnace having hydrogen at a flow rate of 190 ml min^{-1} for 10 h at 400 °C (for POH2, temperature = 700 °C). Reached the room temperature inside the furnace.

XL). SEM images were obtained at different magnifications (up to 12,500×) to decipher features at the nanoscale. The surface functionalization groups on the carbon felt were identified using Fourier-transform infrared spectroscopy FT-IR, (Bruker VERTEX70) in the 400–4000 cm^{-1} range at room temperature using air as sweep gas at 8 ml min^{-1}. The surface fibers of the felts were firstly ground using a mortar and pestle, then diluted in KBr in a weight percent ratio of 1:200 and afterward, placed in the transmission apparatus.

2.4. Electrochemical characterization

2.4.1. Configuration of 3-electrode cell

Cyclic voltammograms (CVs) were retrieved by varying the scan rate from 2.5 mV s^{-1} to 100 mV s^{-1} (2.5, 10, 20, 50, 100 mV s^{-1}) and within the range of −2.4 V to −1.0 V in the configuration of three electrodes cell. A volume of 50 ml of electrolyte A2 was used, 6 mm diameter from each CF sample was placed in a gold tip and submersed in the electrolyte serving as a working electrode. The reference electrode was from Biologic RE-7, filled with 0.01 M $AgNO_3$ + 0.1 M TBAP + acetonitrile, and the counter-electrode was a platinum wire. A Zahner Zennium potentiostat equipped with Thales software enabled the recording of the voltammograms under an inert (N_2) saturated atmosphere. The effect of the purging gas on the electrolyte was studied to verify the stability of V^{3+}/V^{2+} and V^{4+}/V^{3+} redox species and the reversibility of the reactions under an inert (N_2) and oxidative (O_2) environment using a glassy carbon (GC, Metrohm) in the three-electrode cell. An accelerated stress test (AST) was performed to assess the impact of oxygen group functionalities on the surface of the different CFs and screen their impact on the reversibility of the reactions of interest. This protocol encompassed the cycling of the electrodes PO and POH2 from −2.1 V to 1.4 V at 100 mV s^{-1} in N_2 purged electrolyte.

2.4.2. Redox flowcell assembly

The in-house prepared flowcell used in this study was inspired by the configuration of the commercial fuel cell from Pragma Industries. Bipolar plates of graphite fabricated by Roy Carbon containing serpentine flow fields were employed and the remaining sealing materials such as o-rings and gaskets (of Viton and EPDM composition, respectively) were replaced with PTFE material to ensure compatibility with the non-aqueous solvent. The carbon-felt electrodes were sealed inside the cell using Teflon gaskets and then sandwiched between the bipolar plates. An electrode compression of 34 % was applied to the electrode, which corresponds to a thickness of 3 mm. A glove box filled with dry nitrogen was used to perform all of the experiments. Then, 20 ml of electrolyte A1 were circulated through the cell as posolyte and negolyte, at a flow rate of 30 ml min^{-1}, as depicted in Fig. 1. A Zahner workstation, served to perform impedance measurements over the frequency range of 250 kHz to 100 mHz at 10 mV of amplitude and an open circuit potential of $E_{OCP} \cong 1.5$ V. Polarization data was collected at a scan rate of 20 mV s^{-1} in the range of 0.1 V to 2.5 V. Data obtained from charge/discharge cycling (CDC) enabled the calculation of Coulombic, Voltage, and Energy efficiencies (η_{CE}, η_{VE}, and η_{EE}, respectively) for each cycle:

$$\eta_{CE_i} = \frac{\int_{t_{d,0}}^{t_{d,f}} I_d dt}{\int_{t_{c,0}}^{t_{c,f}} I_c dt} \tag{4}$$

$$\eta_{VE_i} = \frac{\int_{t_{d,0}}^{t_{d,f}} E_d(t) dt}{\int_{t_{c,0}}^{t_{c,f}} E_c(t) dt} \times \frac{(t_{c,f} - t_{c,0})}{(t_{d,f} - t_{d,0})} \tag{5}$$

$$\eta_{EE_i} = \eta_{CE_i} \times \eta_{VE_i} \tag{6}$$

where E is denoted as the cell's potential difference; current and time are denoted by I and t; subscript 'i' stands for cycle number; subscript 'c' and 'd' for the charge and discharge, respectively; whereas subscript 0 and 'f' for initial and final cycles.

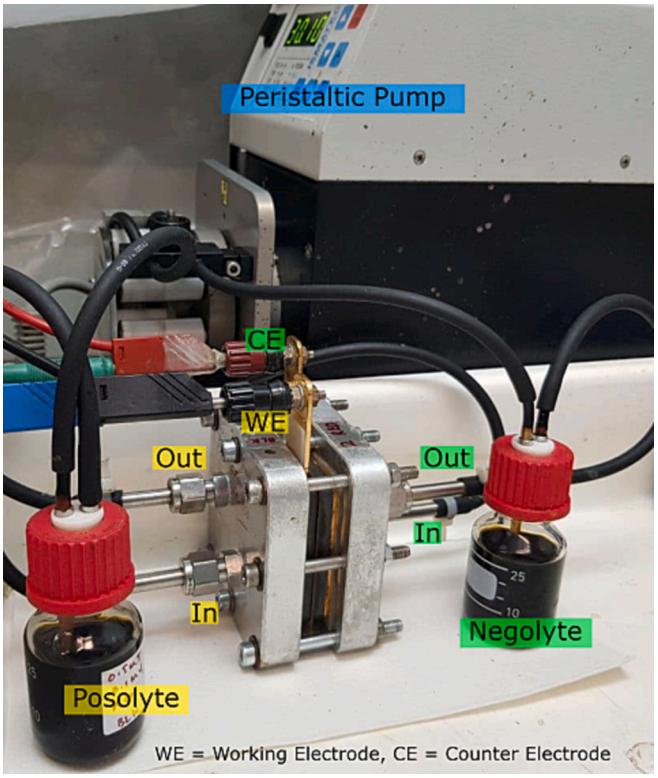

Fig. 1. Experimental setup for a single cell of non-aqueous vanadium redox flow battery. The posolyte and negolyte were pumped at 30 ml min^{-1} from reservoirs by using neoprene tubing. Acronyms: CE = counter electrode, WE = working electrode.

3. Results and discussions

3.1. Effect of environmental moisture and oxygen on the redox species

The non-aqueous electrolyte containing dissolved redox species V $(acac)_3$, was characterized in a three-electrode cell equipped with a glassy carbon performing as a working electrode to screen the electrolyte stability when exposed to oxygen or moisture. The cyclic voltammograms of pristine and contaminated non-aqueous electrolytes are shown in Fig. 2. The cyclic voltammogram of the pristine electrolyte is shown in Fig. 2(a); this voltammogram indicates that the redox reaction is reversible with a cell voltage of 2.2 V. Deionized (DI) water was added gradually to the electrolyte to mimic the increment of relative humidity (RH). The stability of redox pairs – $V^{3+/2+}$ & $V^{4+/3+}$, *cf.* Eqs. (1) and (2) – was assessed in the presence of moisture - Fig. 2(b) and (c). The anodic and cathodic peaks for the redox couple $V^{3+/2+}$ vanished upon the addition of solely 50 ppm DI water. The latter highlights that even the atmospheric moisture - *ca.* RH = 35.6 % @ 25 °C - can degrade the electrolyte, especially, the $V^{3+/2+}$ redox couple. On the other hand, the redox couple of $V^{4+/3+}$ is comparatively less sensitive and therefore, degraded slowly until 2500 ppm - Fig. 2(c); nonetheless, upon the addition of 375,000 ppm, there was an evident peak reduction and even loss of reversibility. The addition of water dilutes the electrolyte which affects the peak current values but the loss achieved surpasses greatly the effect of dilution. Therefore, it is crucial to use a dry atmosphere to keep the electrolyte stable. Since $V^{4+/3+}$ remains stable, it can be used as a posolyte, combined with a suitable negolyte. The proposed reaction mechanism for the parasitic formation of $VO(acac)_2$ is given below [11]:

$$V(acac)_3^{+} + H_2O \rightarrow VO(acac)_2 + Hacac + H^{+} \tag{7}$$

According to Fig. 2(d), additional peaks emerged as a result of the electrolyte being exposed to O_2, indicating a significant influence on the

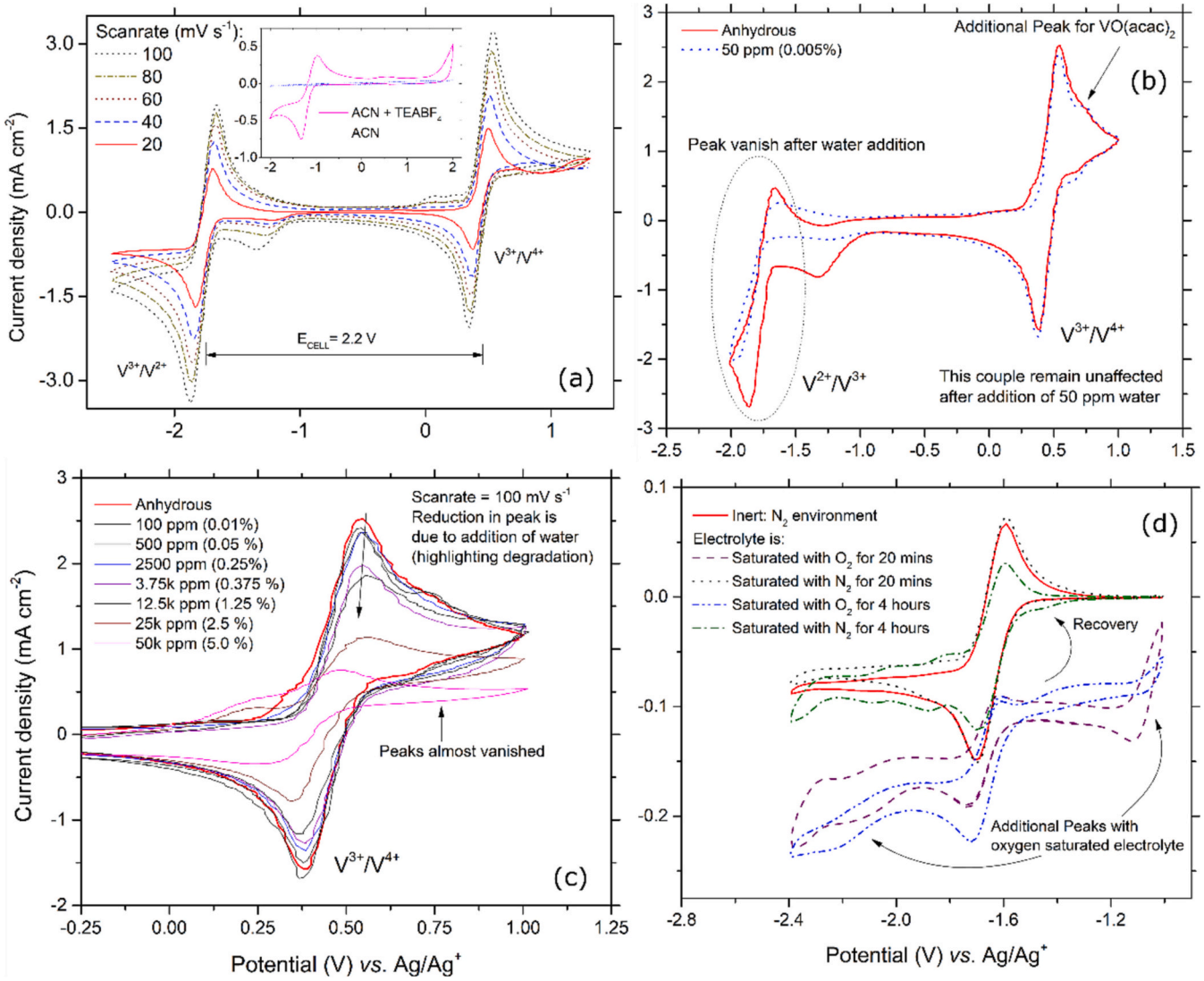

Fig. 2. Voltammogram using 3-electrode cell configuration (a) for the non-aqueous electrolyte using redox species $V(acac)_3$ without any contamination (b) highlighting the effect of gradually adding moisture (water) on the redox couples a) V^{3+}/V^{2+} and V^{4+}/V^{3+} depicting the parasitic product $VO(acac)_2$ (c) V^{4+}/V^{3+} at different moisture concentrations (100 ppm–50k ppm) (d) degradation test was performed from inert nitrogen (N_2) environment to oxygen (O_2) saturation for 20 min and then repeated with saturation for 4 h, first with O_2 and then recovered by N_2.

reaction's shift toward the production of parasitic $VO(acac)_2$. Therefore, maintaining a dry and oxygen-free environment is crucial for a reliable battery operation. Interestingly, it was discovered that the reversibility of the redox species depends on the duration of the exposure to an oxygen source. The impact is minimal for up to 20 min but becomes critically important after 4 h. The aged electrolyte could not be regenerated after 4 h of nitrogen bubbling; the anodic/cathodic peak current densities decreased *ca.* 67 % and additional peaks for $VO(acac)_2$ (−2.1 V and −1.9 V) became apparent in Fig. 2(d). The following reaction mechanism was proposed to happen in parallel with the reduction of molecular oxygen [11]:

$$4V(acac)_3 + 2H_2O + O_2 \leftrightharpoons 4VO(acac)_2 + 4Hacac \quad (8)$$

3.2. Electrochemical surface activity of modified electrodes

The combined thermal treatment of the carbon felt electrodes under an oxygen atmosphere (400 °C, 10 h) followed by a treatment using a hydrogen atmosphere (400 °C, 10 h) was performed to extensively remove the attached oxygen functional groups. An additional set of samples was prepared to assess the impact of the treatment at higher temperatures, 700 °C for 10 h under H_2 flow (samples are named PH2 & POH2). The electrochemical activity of each sample electrode was analyzed by cyclic voltammetry using a three-electrode cell at 25 °C, as detailed in Section 2.4.1. Fig. 3(a) shows the CVs at the scan rate of 10 mV s^{-1} for the samples immersed in V^{3+}/V^{2+} redox couple in the electrolyte having a composition of 0.1 M $TEABF_4$ + 0.02 M $V(acac)_3$ + acetonitrile.

From the spectra plotted in Fig. 3(a), peak currents for $V^{3+/2+}$ are considerably higher for POH electrodes – the anodic peak reaches currents of *ca.* 10.13 mA, followed by carbon felts PO – reaching an anodic peak of 9.53 mA; P and PH electrodes display the worst anodic peak performance. At first glance, these results show that the treatment applied to the POH electrode allows for increasing the number of active sites needed for the redox reaction. Interestingly, the mild oxidative treatment (*i.e.* 400 °C for 10 h under airflow, PO) allows the growth of more surface oxygen functional groups, namely functional groups C═O and C-OH, which appear to demonstrate greater catalytic activity compared to the pristine sample [12]. Fig. 3(b) shows the voltammograms recorded at 10 mV s^{-1}, concerning the impact of increasing the thermal treatment temperature (from 400 °C to 700 °C) during the reduction treatment under H_2 flow. The increase in the thermal

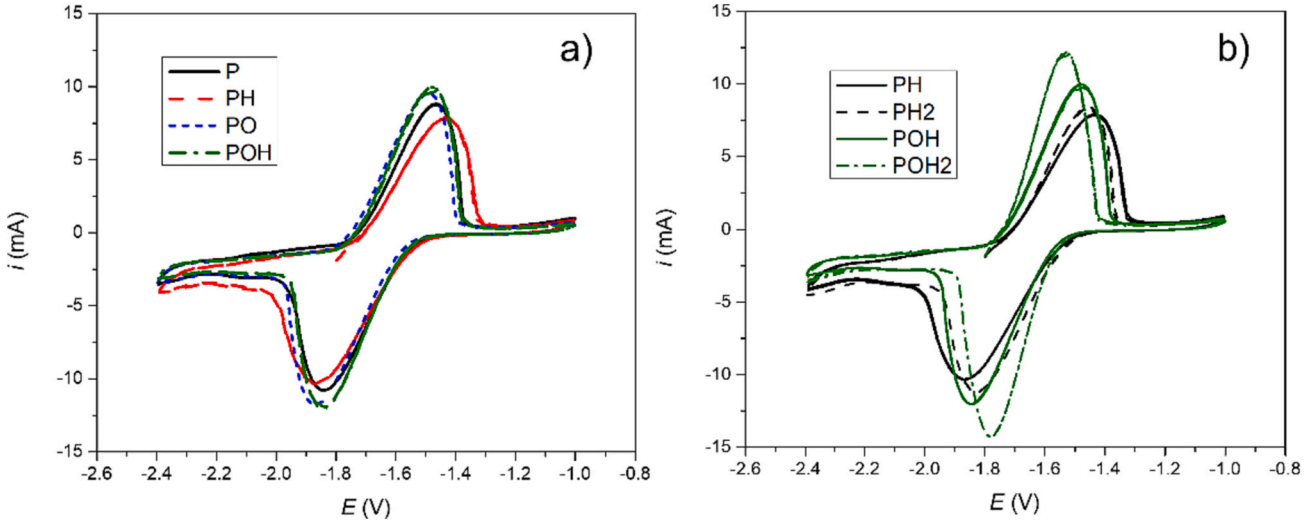

Fig. 3. Cyclic voltammograms at 10 mV s^{-1} for screening the effect of thermal treatment under different environmental conditions a) thermal treatment at 400 °C for the sample electrodes such as pristine (P), pristine + hydrogen (PH), pristine + oxygen (PO), pristine + oxygen + hydrogen (POH); b) the effect of increasing the temperature from 400 °C to 700 °C (PH2, POH2).

treatment temperature modified the surface chemistry to produce more active electrodes (POH2 > POH > PH2 > PH).

Anodic/cathodic peak currents were correlated to the square root of the scan rate, at 25 °C, using the Randles-Sevcik equation. As shown in Fig. S2, nearly for all electrode samples, except for PO, the corresponding current peaks are proportional to the square root of the scan rate as perceived from the obtained linearity. Thereafter, contrarily to the remaining electrodes where the diffusion mechanisms govern entirely the redox reaction mechanism, for the PO electrode, besides diffusion processes, there might be an additional adsorption step governing the redox reaction [13]. The higher slopes from Randles Sevcik plots attributed to the POH2 and POH electrodes - Fig. S3 - are also indications of faster kinetics/mass transfer phenomena.

3.3. Impact of surface modifications on the redox reaction reversibility

To assess the impact of the thermal treatments on the reversibility of the modified carbon felts toward the redox couple, the ratio between the anodic and cathodic peak current densities was examined (I_{pa}/I_{pc}). The redox reaction reversibility is reached as the ratio I_{pa}/I_{pc} approaches the value of 1 [14]. Amongst all the studied CFs, the one displaying the I_{pa}/I_{pc} closer to the unity was POH2 followed by POH, which demonstrates a significant improvement compared to the pristine carbon felt or even comparable to the CF treated under oxygen flow (PO), as shown in Table 2. Additionally, peak-to-peak potential separation ($\Delta E = |E_c - E_a| / n$) analysis provides accurate information about the reversibility of a specific reaction, where high reversibility is indicated by a lower value of the potential separation, ΔE [14,15]. Although the reduced electrodes, such as POH2 (245 mV), PH2 (366 mV), or even POH (370 mV), display the smallest peak-to-peak separation, they still account for irreversible negolyte reactions, since ΔE is larger than the conventional 59 mV [13]. In this regard, insights into the activity of the electrodes can be determined using the reaction rate constant ($K°$) for the oxidation and reduction reactions happening at the negolyte [25]. These details are mentioned in the supplementary information – Fig. S4(a–b) and summarized in Table 2.

A similar trend was observed concerning the thermal treatment of the CFs, where electrodes treated at higher temperature display improved electrochemical reversibility, as evidenced by the smaller value of ΔE of electrodes POH2 and PH2 *vs.* POH and PH, treated respectively at 700 °C and 400 °C. Considering negolyte *i.e.* V^{3+}/V^{2+}, the cell equipped with POH2 electrodes exhibits 5.47 times faster reaction rate compared to the cell equipped with a pristine electrodes, 3.52 cm s^{-1} *vs.* 0.643 cm s^{-1} respectively.

3.4. Electrode stability in the presence of oxygen-rich/less surface

An accelerated stress test (AST) - Fig. S5 - was performed using N_2 purged electrolyte in a three-electrode cell. This test consisted of cycling the potential from −2.1 V to 1.4 V at 100 mV s^{-1} for 700 cycles for both PO and POH2, which are high-performing electrodes during electrochemical analysis. The main goal is to assess whether the presence of pseudocapacitive oxygen groups on the surface of the carbon hinders the electrochemical reversibility of the reaction of interest as the environment is completely oxygen-free and therefore solely the oxygen functional groups on the CF surface will be responsible for causing any performance loss. Moreover, the potential was cycled until such positive potentials - up to 1.4 V - to mimic the potential at which the irreversible species forms, typically – 0.75 *vs.* Ag/Ag^+ [9,16], *cf.* Eqs. (7) and (8)– and thus, allow to identify the electrode more prone for developing VO $(acac)_2$ parasitic species.

From Fig. 4(a), it can be observed that there is a drop of nearly 46 % in the I_{pa}/I_{pc} ratio for the PO electrode as compared to solely *ca.* 20 % for the POH2 electrode – after 700 cycles which corresponds to *ca.* 20 h.

Table 2
Summary of electrochemical parameters determined for each sample electrode using cyclic voltammetry at 10 mV s^{-1} having the non-aqueous electrolyte.

Electrode type	I_{pa} (mA)	I_{pc} (mA)	E_{pa} (V)	E_{pc} (V)	I_{pa}/I_{pc}	ΔE (mV)	K^0_A (cm s^{-1}) oxidation	K^0_C (cm s^{-1}) reduction × 10^{-3}
P	8.5	10.26	−1.46	−1.85	0.83	385	0.643	2.3
PH	7.92	10.35	−1.44	−1.86	0.77	422	0.391	4.79
PH2	8.43	10.57	−1.46	−1.83	0.80	366	0.570	3.05
PO	9.53	11.77	−1.49	−1.88	0.81	386	1.74	0.620
POH	10.13	12.09	−1.48	−1.85	0.84	370	1.64	0.150
POH2	12.10	14.19	−1.53	−1.78	0.85	245	3.52	0.650

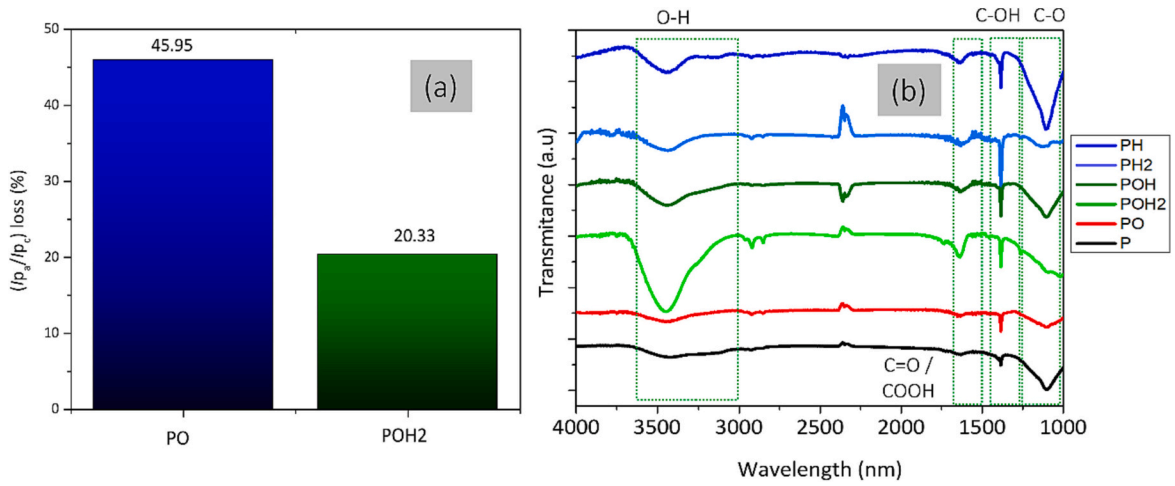

Fig. 4. (a) Loss of reversibility (I_{pa}/I_{pc}) ratio after AST for PO and POH2. (b) FTIR was performed on samples of carbon felt. Legend: Pristine (P), pristine + oxygen treatment (PO), pristine + hydrogen treatment at 400 °C (PH), pristine + hydrogen treatment at 700 °C (PH2), PO + hydrogen treatment at 400 °C (POH), and PO + hydrogen treatment at 700 °C (POH2).

Besides, by analyzing the peak-to-peak separation data (ΔE) from Table 3, it is observed that upon the accelerated stress test, the ΔE appears diminished at the end of the test (25 % for PO and 34 % for POH2), and it is due to the creation of additional surface defects or higher porosity from the repetitive cycling [17]. Besides that, the reaction rate constant, K^0_A, for PO after degradation (PO-AST) utterly drops and achieved a lower value compared to POH2 after the AST (*i.e.*, 0.85 cm s^{-1} *vs.* 1.06 cm s^{-1}, respectively).

The presented results highlight that the surplus of oxygen-containing groups at the carbon felts surfaces hinders the performance of non-aqueous RFB, despite these functional oxygen groups being generally considered to improve the performance of the aqueous RFB [18]. For the proposed non-aqueous RFB technology, the presence of such groups triggers the formation of parasitic $VO(acac)_2$, strongly hindering both the battery's stability and capacity.

3.5. Morphology characterization applied to prepared electrodes

Morphology characterizations were performed to assess the effect of hydrogen/oxygen treatment on the surface chemistry of the carbon felts. FT-IR spectra of the various treated carbon felts are shown in Fig. 4(b). All carbon felt samples show four similar bands; a strong band attributed to the stretching vibration of (C—O) groups in the region between ~1200 and 1100 cm^{-1} related to alcohol/phenol groups. A broader band appearing in the range of 1470–1380 cm^{-1} is due to a series of overlapping absorption bands related to the deformation vibration of surface hydroxyl groups (C-OH) and in-plane vibrations of C—H in several C=C-H structures; these are considered as typical for carbon materials. In the region of ~1620 to 1600 cm^{-1}, a band originated due to the conjugated C=C stretching vibrations and carbonyl (C=O) groups [19].

In the spectra of the carbon materials, the band of stretching vibrations (3600–3100 cm^{-1}) was due to surface hydroxylic groups (O—H) and vibration modes from the moisture adsorbed on the sample [20]. The strong broader peaks for samples pristine (P) and air/oxidation treatment (PO) are due to the superposition of the vibration of hydroxyl groups that arise when the carbon is highly oxidized [21]. The latter indicates that the heat treatment under an atmosphere of oxygen at 400 °C allowed to increase in the amount of oxygen functional groups in the carbon felts which is evident from the broader bands in the region of 3600–3100 cm^{-1}. Whereas, the samples that were reduced in hydrogen (PH, PH2, POH, and POH2) show narrower peaks and thus are likely to have fewer amount of surface OH groups.

SEM characterizations of all the sample electrodes are shown in Fig. 5. There are noticeable differences - Fig. 5(a) to (c) - between the pristine electrodes, samples PH and PH2. The pristine carbon felt shows a pronounced grooved and coarse surface. The treatment using the hydrogen atmosphere at 400 °C and 700 °C originated a clean and smooth homogeneous surface. Electrodes that were previously subjected to a soaking step in sulfuric acid - PO, POH, and POH2 - display roughened fibers with larger surface area, as can be confirmed by the greater higher peak currents obtained – *cf.* Fig. 3. Most likely, the chemical treatment is harsh for the surface, generating too many defects. The acid treatment followed by thermal treatments, firstly under airflow and secondly under hydrogen flow, generate additional porosity onto the fibers, which is apparent from the significant increase in the amount of dark large dots in Fig. 5(e). Nonetheless, the corresponding sample treated at 700 °C *i.e.* for POH2, seems to have a smoother surface. Oxidative thermal treatments are generally performed to increase the number of oxygen functional groups. By applying a thermal treatment in an oxygen environment followed hydrogen environment, it is expected that these functional groups are removed and many surface defects are created – *i.e.* for POH, POH2. These expectations confirm the precedence set by FTIR analysis - Fig. 4(b) and electrochemical analysis (Fig. S4).

Table 3
Summary of electrochemical parameters determined by CV for PO and POH2 CFs for V^{3+}/V^{2+} redox couple at the beginning of life (BoL) and upon the AST/ stability test.

	I_{pa} (mA)	I_{pc} (mA)	E_{pa} (V)	E_{pc} (V)	I_{pa}/I_{pc}	ΔE (mV)	K^0_A (cm s^{-1}) oxidation
PO BoL	9.53	11.77	−1.49	−1.88	0.81	386	1.74
PO AST	4.551	10.46	−1.53	−1.82	0.44	290	0.85
POH2 BoL	12.10	14.19	−1.53	−1.78	0.85	245	3.52
POH2 AST	6.169	9.08	−1.57	−1.73	0.68	162	1.06

Acronyms: BoL = beginning of life, AST = accelerated stress test.

3.6. Performance of the redox flow cell

Charge/discharge cycling (CDC) is a key electrochemical test to assess the performance of the NAqRFB-cell assembled with the electrodes here in the study. A recent article reports a NAqRFFB-cell with similar electrochemistry, tested at a C-rate of 0.2C [22]. To assess the performance of the cell at a higher current density, it was considered a higher C-rate of 1.35C (where C is the nominal capacity of the cell *ca.* 33.5 mAh). This corresponds to a larger discharge rate of 6.2 mA cm^{-2}.

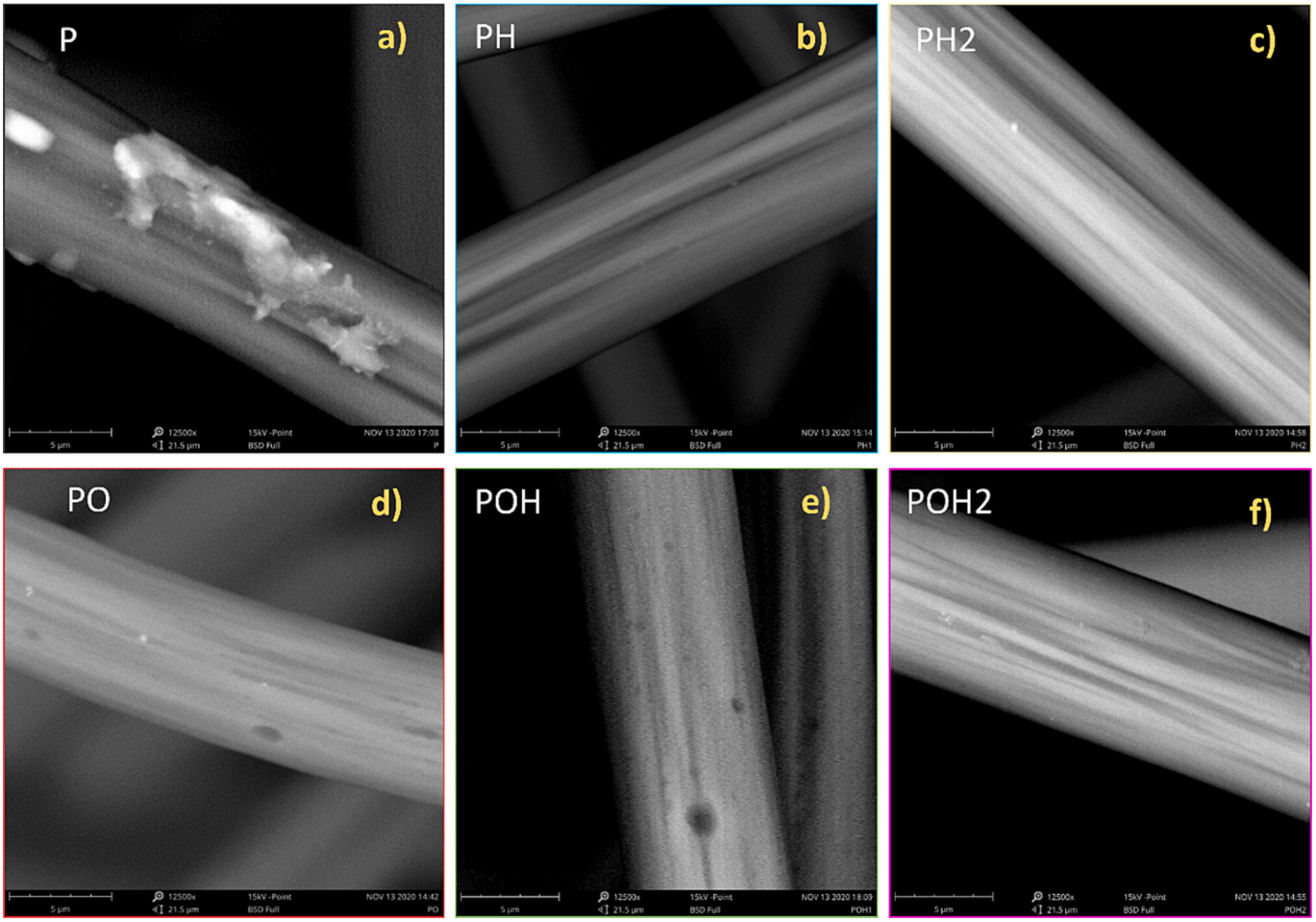

Fig. 5. SEM images of carbon felts at 12,500×; a) pristine (P), b) pristine + hydrogen treatment at 400 °C (PH), c) pristine + hydrogen treatment at 700 °C (PH2), d) pristine + oxygen treatment (PO) d), PO + hydrogen treatment at 400 °C (POH), and f) PO + hydrogen treatment at 700 °C (POH2).

Composite membranes, bipolar plates, current collectors, and flow conditions were kept the same throughout this study.

The performance of the cell equipped with each pair of sample electrodes is shown in Fig. 6. The performance of pristine electrodes – P – was taken as a reference for comparison purposes. Overall, the electrode samples treated under a hydrogen atmosphere display a better performance compared to the results of pristine electrodes and PO electrodes. Interestingly, the coulombic efficiency – η_{CE} – of PO surpasses that of the pristine – P – sample after 30 charge/discharging cycles (CDC), whereas the capacity of the cell reaches solely a rather negligible 2.0 mAh – Fig. 6(a). This steep drop upon solely 10 CDC – Fig. 6(d) – was assigned to the formation of the parasitic species - VO $(acac)_2$ - due to the reaction triggered between redox species and the oxygen functional groups at the microstructure of carbon felts.

Electrode PO also displays a larger number of defects due to larger peak current densities attained compared with electrodes PH and PH2 – Fig. 3. This is also evident here by the cell equipped with electrode PO which initially reaches a higher capacity of *ca.* 23 mAh but steeply drops to *ca.* 0.25 mAh by the 45th cycle. The behavior of the cell equipped with PO electrodes is similar to the results obtained for the 3-electrode cell; the peak current density of both anodic and cathodic was initially higher but when exposed to the accelerated aging experiment, the reversibility of the reaction dropped significantly to *ca.* 46 % (*cf.* Fig. 4). This supports the thesis that the parasitic vanadyl precipitates are formed due to the surface chemistry of the carbon felt, which is rich in oxygen functional groups. The formation of greenish crystal precipitates was also observed at the surface of the PO *post-mortem* electrodes, as shown in Fig. S8. Upon further investigations, it was found that the solubility of $VO(acac)_2$ is 0.06 M in acetonitrile [11], which is significantly lower as compared to $V(acac)_3$, and hence, $VO(acac)_2$ easily precipitates [23].

Moreover, this unexpected overlayer of $VO(acac)_2$ causes 6-fold higher (from *ca.* 2.5 Ω to 15 Ω) charge transfer resistance at the PO electrode, which is noticeable in the EIS spectra – Fig. 7(b) – recorded at 1.5 V after the CDC. In this regard, it is possible to confirm that the presence of an oxygen-rich electrode sparks the generation of $VO(acac)_2$, parasitic species, which blocks the active sites of the electrode making the charge transfer resistance increase substantially. Ohmic resistance also increases for PO with CDC due to the presence of such parasitic precipitates at the surface of the PO electrode and deposition on the membrane surface, which condemns both ionic conductivity and increases interfacial contact resistance of the cell – *cf.* Fig. 7(a) inset *vs.* Fig. 7(b) inset. No precipitates were observed for the remaining *post-mortem* analysis of electrodes that were treated in a hydrogen atmosphere. The higher overall PO impedance entails the lowest voltage (η_{VE}) and energy efficiencies (η_{EE}) attained.

The cell assembled with PH electrodes displays a coulombic efficiency of $\eta_{CE} = 98$ %, a voltage efficiency of $\eta_{VE} = 58$ %, and an energy efficiency of $\eta_{EE} = 57$ %, which is similar to the cell equipped with POH electrodes. Still, the average storage capacity of the cell equipped with PH electrodes is *ca.* 6.14 mAh, which is poorer than the cell performance equipped with POH2 electrodes, which is *ca.* 10.42 mAh, yet still providing a fairly stable operation. This indicates that the oxygen-free electrodes are beneficial to increasing the stability of the cell. A lower

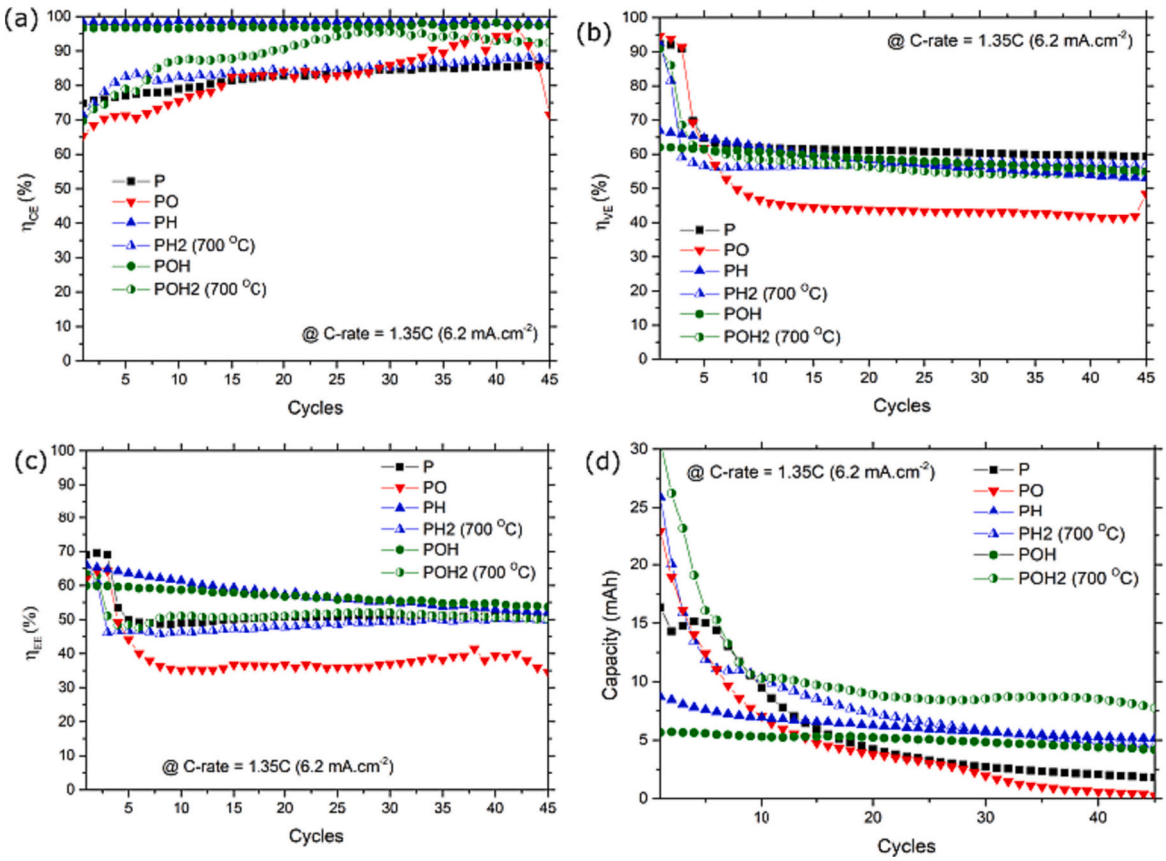

Fig. 6. Performance of V-NAqRFB assembled with prepared electrodes operating at the flow rate of 30 ml min^{-1} at the C-rate of 1.35C *i.e.* 6.2 mA cm^{-2} (a) Coulombic efficiency (η_{CE}) (b) voltage efficiency (η_{VE}) (c) energy efficiency (η_{EE}) (d) capacity for each cycle.

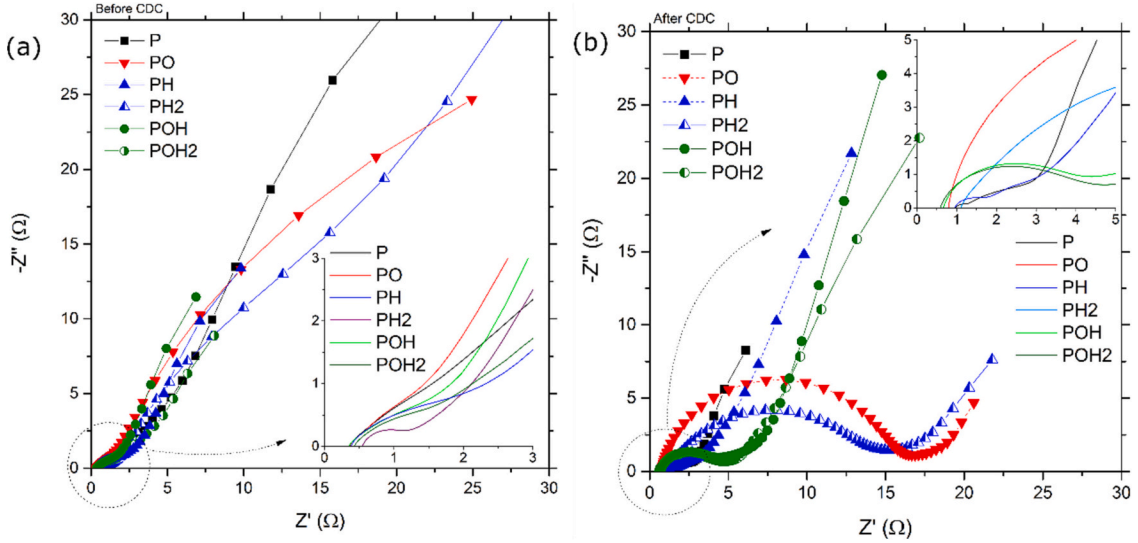

Fig. 7. Impedance curves were obtained through electrochemical impedance spectroscopy performed at $E_{OCP} = 1.5$ V from 250 kHz to 100 mHz with an amplitude of 10 mV. (a) Performed before charge-discharge cycling (b) performed after charge-discharge cycling.

value of the capacity was expected for the cell equipped with PH electrodes because they displayed the lowest number of defects – *i.e.* lower anodic/cathodic peak currents Fig. 3, and lower reaction rate constants (K_A^0), Fig. S4. Increasing the temperature of the H_2 reduction treatment boosted the K_A^0 and therefore, both PH2 and POH2 electrodes exhibit a higher capacity compared with their counterparts, PH and POH, as seen in Fig. 6(d).

A thermal treatment with only hydrogen reduces the manufacturing steps to produce oxygen-less electrodes, however, the POH2 electrode is the one that displayed the best performance. The acid treatment followed by oxygen treatment generates large amounts of surface defects and abundant oxygen functional groups. These latter groups are then reduced under a hydrogen atmosphere at 700 °C. Although the energy efficiency of the cell using POH2 electrodes ($\eta_{EE} = 52$ %) falls behind the

one using POH electrodes (η_{EE} = 56 %), it achieved much higher capacity during the initial cycles (*ca.* 30 mAh) stabilizing afterward, at almost twice the value compared to POH – *cf.* Fig. 6(d). Furthermore, the ohmic resistance – R_Ω – increase between cycle 0th and cycle 45th - Table S1 - is smaller for the cell using POH2 (*ca.* 43 %) and POH (*ca.* 91 %) electrodes compared with pristine (*ca.* 162 %) and for PO (*ca.* 123 %) electrodes. A lower ohmic resistance increase implies that the graphitization level of the POH2 electrode was higher which contributes to an enhanced electrical contact between the electrode surface and the bipolar plates, *cf.* Fig. 7. Moreover, the increment in R_Ω, which is common to all electrodes, was assigned to the degradation of the Nafion composite membrane – C25-HP-C25. A previous work denoted the importance of using separators to minimize the crossover effects of vanadium V^{2+} species and to reduce the degradation effects [8].

The highest limiting current density - Fig. 8 - was achieved with POH2 (*ca.* 104 mA cm^{-2}) followed by PH2 (*ca.* 93 mA cm^{-2}). These values correspond to a C-rate = 22C and 20C respectively, where C is 33.5 mAh – nominal capacity. This highlights that cells equipped with electrode POH2 are capable to be operated at the largest to-date reported limiting current density for this system – 104 mA cm^{-2}.

The state-of-the-art and highest current density is *ca.* 100 mA cm^{-2} for a similar electrochemical system was reported by J. Saraidaridis [24]. These authors assigned the observed current density to the strict control of environmental moisture in the glovebox (max. 250 ppm of humidity) and further to the supply of the chemicals, *i.e.* the credit was given to the good sealing of the bottles that contained the chemicals, from Strem in the UK, as compared to Sigma Aldrich. Good sealing of the bottles helps to prevent the formation of vanadyl, which is a parasitic species. Furthermore, the second-highest performing V-NAqRFB, which was operated by I.L. Escalante-García [9], achieved merely 10 mA cm^{-2} under similar conditions; yet, these authors observed an enormous capacity loss of 90 % after solely 10 CDC, despite having run the experiments inside a glove-box (max. 250 ppm of humidity) and using electrolytes of high purity. The only major difference between both studies is the pre-treatment applied to the electrodes. J. Saraidaridis et al. [24] used carbon-felt electrodes treated at 250 °C for 48 h under a vacuum, while, I.L. Escalante-García [9] used as-received electrodes without any treatment. These results support the conclusions of the present study, *i.e.* the parasitic species are formed from the oxygen functional groups present in the electrodes. It should be emphasized that the glove box used in our laboratory contained *ca.* 6000 ppm of humidity and 100 ppm of oxygen, which highlights that the effect of electrodes is far more relevant than the environmental conditions [26]. The conclusions of this work enable the easy preparation of electrodes using standard industrial processes and motivate researchers to move one step closer to the implementation of a vanadium-based non-aqueous redox flow battery as a promising technology for energy storage.

4. Conclusion

The non-aqueous redox flow battery was studied using vanadium acetylacetonate $V(acac)_3$ as a model redox species. These redox species are commercially available at a reasonable price and are more soluble in non-aqueous solvents in comparison to most organic solvents. Nevertheless, merits frequently come with some drawbacks. Moisture and/or oxygen in the environment induces the formation of parasitic species $VO(acac)_2$, which leads to a rapid loss in battery capacity. The electrolyte must therefore be stored in an inert environment, such as dry nitrogen. Nonetheless, it was observed that even by keeping a strictly controlled inert environment, the stability of the batteries was still rather low. A prominent loss was observed in the anodic/cathodic peak current densities to *ca.* 67 % and a rise of additional redox peaks (at −2.1 V, −1.9 V, and 0.75 V *vs.* Ag^+/Ag) after bubbling the electrolytes with oxygen and after adding DI water in a 3 electrode-configuration cell. This study proposes for the first time that carbon felt electrodes contribute as a major source of oxygen that triggers parasitic reactions since their surface is typically enriched in oxygen group functionalities.

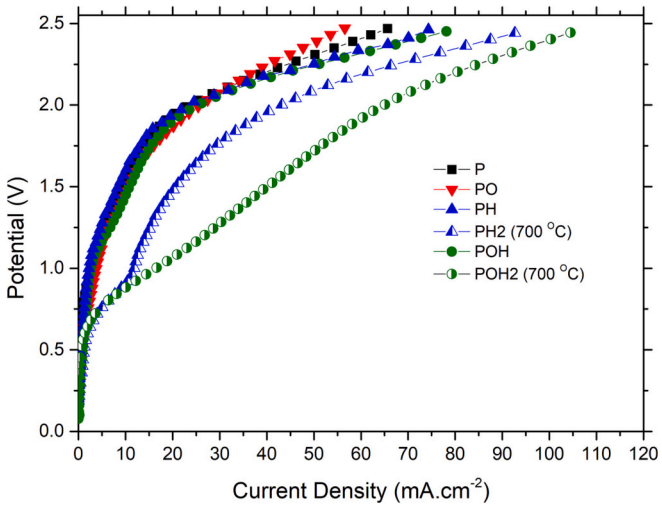

Fig. 8. Polarization curves were obtained while linear sweeping in the range of 0.1 V to 2.5 V at the scan rate of 20 mV s^{-1} and electrolyte flowing at 30 ml min^{-1}.

The carbon felt electrodes were then submitted to a set of different treatments for removing these oxygen functional groups to increase the surface area (morphology). The best performance was obtained when the electrodes were treated at 400 °C under oxygen, followed by a treatment at 700 °C under hydrogen atmosphere – POH2 sample. The cell equipped with POH2 electrodes outperformed all those reported in the literature for similar systems, achieving efficiencies of *ca.* η_{CE} = 90 %, η_{VE} = 57 %, and η_{EE} = 52 %. More importantly, the capacity of the cell remained stable at *ca.* 10.42 mAh and also achieved the highest reported limiting current density of *ca.* 104 mA cm^{-2}.

The results of this work highlight the critical relevance of the chemisorbed oxygen at the surface of the carbon electrodes for the performance of the vanadium NAqRFB; oxygen-free electrodes or electrodes containing inert oxygen functional groups should be used. Since the chemisorbed oxygen functional groups are quite important for allowing the redox species to anchor and exchange electrons at the electrode surface, research should progress on assessing the effect of inert carbon surface dopants, where nitrogen appears as a very promising candidate.

CRediT authorship contribution statement

Kashif Mushtaq: Conceptualization, Methodology, Investigation, Writing – original draft, Visualization. **Sofia Delgado:** Investigation, Writing – review & editing, Visualization. **Adelio Mendes:** Resources, Supervision, Funding acquisition, Writing – review & editing.

Declaration of competing interest

The authors declare that they have no known competing financial interests or personal relationships that could have appeared to influence the work reported in this paper.

Acknowledgments

This work was financially supported by the base funding from the Laboratory for Process Engineering, Environment, Biotechnology, and Energy – LEPABE having reference number UIDB/00511/2020. The national funds support this work through the Fundação para a Ciência e a Tecnologia – FCT; Ministério da Ciência, Tecnologia e Ensino Superior – MCTES; Programa de Investimentos e Despesas de Desenvolvimento da Administraçãao Central – PIDDAC, and FEDER funds through

COMPETE2020 - Programa Operacional Competitividade e Internacionalizaçao – POCI. The projects related to this work are POCI-01-0145-FEDER-016387 – SunStorage, POCI-01-0145-FEDER-030510 – Sunflow, POCI-01-0145-FEDER-030223 – Polysol, POCI-01-0247-FEDER-046109 – Batteries 2030 and POCI-01-0247-FEDER-046846 – BluEnergy. Kashif Mushtaq acknowledges the Massachusetts Institute of Technology Portugal Program – MITPP; and FCT for the doctoral grant having reference number PD/BD/128041/2016. Sofia Delgado acknowledges FCT for the doctoral grant having reference number SFRH/BD/144338/2019.

Appendix A. Supplementary data

Supplementary data to this article can be found online at https://doi.org/10.1016/j.est.2023.108593.

References

[1] Eu, Estimated CO_2 Emissions From Energy Use Share of EU Total CO2 Emissions in 2017, 2017.
[2] Forecasted electric vehicle battery demand worldwide, Statista, 2020. https://www.statista.com/statistics/1129463/forecasted-electric-vehicle-battery-demand-worldwide/. (Accessed 28 July 2021).
[3] O. Schmidt, S. Melchior, A. Hawkes, I. Staffell, Projecting the future levelized cost of electricity storage technologies, Joule. 3 (2019) 81–100, https://doi.org/10.1016/j.joule.2018.12.008.
[4] S. Roe, C. Menictas, M. Skyllas-Kazacos, A high energy density vanadium redox flow battery with 3 M vanadium electrolyte, J. Electrochem. Soc. 163 (2016) A5023–A5028, https://doi.org/10.1149/2.0041601jes.
[5] M. O, N. Pour, Y. Shao-Horn, S. Almheiri, Systematic selection of solvent mixtures for non-aqueous redox flow batteries – vanadium acetylacetonate as a model system, Electrochim. Acta 223 (2017) 115–123, https://doi.org/10.1016/j.electacta.2016.12.014.
[6] J. Friedl, M.V. Holland-Cunz, F. Cording, F.L. Pfanschilling, C. Wills, W. McFarlane, B. Schricker, R. Fleck, H. Wolfschmidt, U. Stimming, Asymmetric polyoxometalate electrolytes for advanced redox flow batteries, Energy Environ. Sci. 11 (2018) 3010–3018, https://doi.org/10.1039/c8ee00422f.
[7] P. Geysens, Y. Li, I. Vankelecom, J. Fransaer, K. Binnemans, Highly soluble 1,4-diaminoanthraquinone derivative for nonaqueous symmetric redox flow batteries, ACS Sustain. Chem. Eng. 8 (2020) 3832–3843, https://doi.org/10.1021/acssuschemeng.9b07244.
[8] K. Mushtaq, T. Lagarteira, A.A. Zaidi, A. Mendes, In-situ crossover diagnostics to assess membrane efficacy for non-aqueous redox flow battery, J. Energy Storage 40 (2021) 102713–102722, https://doi.org/10.1016/j.est.2021.102713.
[9] I.L. Escalante-García, J.S. Wainright, L.T. Thompson, R.F. Savinell, Performance of a non-aqueous vanadium acetylacetonate prototype redox flow battery: examination of separators and capacity decay, J. Electrochem. Soc. 162 (2015) A363–A372, https://doi.org/10.1149/2.0471503JES.
[10] K.J. Kim, S.-W. Lee, T. Yim, J.-G. Kim, J.W. Choi, J.H. Kim, M.-S. Park, Y.-J. Kim, A new strategy for integrating abundant oxygen functional groups into carbon felt electrode for vanadium redox flow batteries, Sci. Rep. 4 (2014) 1–6, https://doi.org/10.1038/srep06906.
[11] A.A. Shinkle, A.E.S. Sleightholme, L.D. Griffith, L.T. Thompson, C.W. Monroe, Degradation mechanisms in the non-aqueous vanadium acetylacetonate redox flow battery, J. Power Sources (2012) 490–496, https://doi.org/10.1016/j.jpowsour.2010.12.096 (Elsevier).
[12] K.J. Kim, Y.J. Kim, J.H. Kim, M.S. Park, The effects of surface modification on carbon felt electrodes for use in vanadium redox flow batteries, Mater. Chem. Phys. 131 (2011) 547–553, https://doi.org/10.1016/j.matchemphys.2011.10.022.
[13] N. Elgrishi, K.J. Rountree, B.D. McCarthy, E.S. Rountree, T.T. Eisenhart, J. L. Dempsey, A practical beginner's guide to cyclic voltammetry, J. Chem. Educ. 95 (2018) 197–206, https://doi.org/10.1021/acs.jchemed.7b00361.
[14] P. Han, Y. Yue, Z. Liu, W. Xu, L. Zhang, H. Xu, S. Dong, G. Cui, Graphene oxide nanosheets/multi-walled carbon nanotubes hybrid as an excellent electrocatalytic material towards VO 2+/VO 2+ redox couples for vanadium redox flow batteries, Energy Environ. Sci. 4 (2011) 4710–4717, https://doi.org/10.1039/c1ee01776d.
[15] M. Park, Y. Jung, J. Kim, H. Il Lee, J. Cho, Synergistic effect of carbon nanofiber/nanotube composite catalyst on carbon felt electrode for high-performance all-vanadium redox flow battery 13 (2013) 5, https://doi.org/10.1021/nl402566s.
[16] Q. Liu, A.E.S. Sleightholme, A.A. Shinkle, Y. Li, L.T. Thompson, Non-aqueous vanadium acetylacetonate electrolyte for redox flow batteries, Electrochem. Commun. 11 (2009) 2312–2315, https://doi.org/10.1016/j.elecom.2009.10.006.
[17] K.V. Greco, A. Forner-Cuenca, A. Mularczyk, J. Eller, F.R. Brushett, Elucidating the nuanced effects of thermal pretreatment on carbon paper electrodes for vanadium redox flow batteries, ACS Appl. Mater. Interfaces 10 (2018) 44430–44442, https://doi.org/10.1021/acsami.8b15793.
[18] K. Kim, S.W. Lee, T. Yim, et al., A new strategy for integrating abundant oxygen functional groups into carbon felt electrode for vanadium redox flow batteries, Sci. Rep. 4 (2014) 6906, https://doi.org/10.1038/srep06906.
[19] B. Manoj, A.M. Raj, G.C. Thomas, Tailoring of low grade coal to fluorescent nanocarbon structures and their potential as a glucose sensor, Sci. Rep. 8 (2018) 13891, https://doi.org/10.1038/s41598-018-32371-9.
[20] X. Huang, N. Hu, R. Gao, Y. Yu, Y. Wang, Z. Yang, E. Siu-Wai Kong, H. Wei, Y. Zhang, Reduced graphene oxide-polyaniline hybrid: preparation, characterization and its applications for ammonia gas sensing, J. Mater. Chem. 22 (2012) 22488–22495, https://doi.org/10.1039/c2jm34340a.
[21] J. Yang, Y. Wang, J. Wang, M.B. Chan-Park, Reducing graphene oxide with a modified Birch reaction, RSC Adv. 5 (2015) 11124–11127, https://doi.org/10.1039/c4ra13801e.
[22] S. on Tung, S.L. Fisher, N.A. Kotov, L.T. Thompson, Nanoporous aramid nanofibre separators for nonaqueous redox flow batteries, Nat. Commun. 9 (2018), https://doi.org/10.1038/s41467-018-05752-x.
[23] L. Guglielmero, M.M. Langroudi, M. Al Khatib, M.A.C. de Oliveira, B. Mecheri, M. De Leo, A. Mezzetta, L. Guazzelli, R. Giglioli, A.D. Epifanio, R. Pogni, C. Chiappe, C.S. Pomelli, Electrochemical and spectroscopic study of vanadyl acetylacetonate–ionic liquids interactions, Electrochim. Acta 373 (2021), 137865, https://doi.org/10.1016/j.electacta.2021.137865.
[24] J.D. Saraidaridis, C.W. Monroe, Nonaqueous vanadium disproportionation flow batteries with porous separators cycle stably and tolerate high current density, J. Power Sources 412 (2019) 384–390, https://doi.org/10.1016/j.jpowsour.2018.11.058.
[25] A.Ya. Gokhshtein, Kinetic equation of irreversible reactions in oscillographic polarography, Dokl. Akad. Nauk SSSR 131 (3) (1960) 601–604. http://www.mathnet.ru/php/archive.phtml?wshow=paper&jrnid=dan&paperid=39925&option_lang=eng. (Accessed 19 October 2021) (n.d.).
[26] K. Mushtaq, S. Delgado, A. Mendes, Nanoparticles enrichment to carbon felt electrodes for non-aqueous redox flow battery, J. Energy Storage. ISSN: 2352-152X 65 (2023) 107234, https://doi.org/10.1016/j.est.2023.107234. https://www.sciencedirect.com/science/article/pii/S2352152X2300631X.

Glossary

EBV: Electric battery vehicles
LIB: Li-ion batteries
LCOS: lowest levelized cost of storage
NiMH: Nickel metal hydride
Ni-Cd: Nickel cadmium
T_{atm}: Atmospheric temperature
P_{atm}: Atmospheric pressure
RFB: Redox flow batteries
V-NAqRFB: Vanadium non-aqueous redox flow battery
SEM: Scanning electron microscopy
FTIR: Fourier-transform infrared spectroscopy
CV: Cyclic voltammetry
AST: Accelerated stress test
PTFE: Poly-tetra-fluoro-ethylene
CDC: Charge-discharge cycling
DI: Deionized water
RH: Relative humidity
WE: Working electrode
CE: Counter electrode
RE: Reference electrode
P: Pristine
PO: Pristine with thermal treatment in O_2 environment
POH: Pristine with thermal treatment in O_2 followed by H2 at 400 °C
POH2: Pristine with thermal treatment in O_2 followed by H2 at 700 °C
PH: Pristine with thermal treatment in H_2 environment at 400 °C
PH2: Pristine with thermal treatment in H_2 environment at 700 °C